

FEAST EIGENSOLVER FOR NON-HERMITIAN PROBLEMS

JAMES KESTYN*, ERIC POLIZZI†, AND PING TAK PETER TANG‡

Abstract. A detailed new upgrade of the FEAST eigensolver targeting non-Hermitian eigenvalue problems is presented and thoroughly discussed. It aims at broadening the class of eigenproblems that can be addressed within the framework of the FEAST algorithm. The algorithm is ideally suited for computing selected interior eigenvalues and their associated right/left bi-orthogonal eigenvectors, located within a subset of the complex plane. It combines subspace iteration with efficient contour integration techniques that approximate the left and right spectral projectors. We discuss the various algorithmic choices that have been made to improve the stability and usability of the new non-Hermitian eigensolver. The latter retains the convergence property and multi-level parallelism of Hermitian FEAST, making it a valuable new software tool for the scientific community.

Key words. non-Hermitian eigenproblem, FEAST, spectral projectors, contour integration, right/left eigenvectors, bi-orthogonal vectors

AMS subject classifications. 65F15, 15A18 34L16 65Y05 35P99

1. Introduction. The generalized eigenvalue problem $AX = BX\Lambda$ with A and B square matrices and Λ diagonal, is a central topic in numerical linear algebra and arises from a broad and diverse set of disciplines in mathematics, science and engineering (the problem is said “standard” if $B \equiv I$ or “generalized” otherwise). Solving the interior eigenvalue problem consists of determining nontrivial solutions $\{\lambda_i, x_i\}$ (i.e. eigenpairs with $x_i = Xe_i$ and $\lambda_i = \Lambda_{i,i}$) located anywhere inside the spectrum. Most common numerical applications lead to symmetric eigenvalue problems where A is real symmetric or complex Hermitian, B is symmetric or Hermitian positive definite (hpd), and all the obtained eigenvalues λ_i are real. Non-symmetric and non-Hermitian eigenvalue problem (including the case where A is complex symmetric) can also be encountered in a variety of situations resulting in complex values for λ_i . In this case x_i is called the right eigenvector associated with λ_i , while one can also define a left eigenvector $\hat{x}_i = \hat{X}e_i$ solution of $\hat{X}^H A = \Lambda \hat{X}^H B$ (i.e. $A^H \hat{X} = B^H \hat{X} \Lambda^*$). Although many software packages are available for symmetric (or Hermitian) matrices (see e.g. [17, 23, 33, 18, 25, 5, 36, 20]), relatively few algorithms and software can handle the non-Hermitian problem [22, 4, 23, 3, 13]. The FEAST eigensolver [29, 10], proven to be a robust and efficient tool for computing the partial eigenspectrum of Hermitian system matrices [38], can also be generalized and applied to arbitrary non-Hermitian systems [21, 41, 37].

FEAST is a subspace iteration method that uses the Rayleigh-Ritz projection and an approximate spectral projector as a filter [38]. Given a Hermitian generalized eigenvalue problem $AX = BX\Lambda$ of size n , the algorithm in Figure 1 outlines the main steps of a generic Rayleigh-Ritz subspace iteration procedure for computing m eigenpairs. At convergence, the algorithm yields the B -orthonormal eigensubspace $Y_m \equiv X_m = \{x_1, x_2, \dots, x_m\}_{n \times m}$ and associated eigenvalues $\Lambda_{Q_m} \equiv \Lambda_m$. Taking $\rho(B^{-1}A) = B^{-1}A$, yields the bare-bone subspace iteration (generalization of the power method) which converges towards the m dominant eigenvectors with the linear rate $|\lambda_{m_0+1}/\lambda_i|_{i=1, \dots, m}$ [31, 32, 28]. This standard approach is never used in practice.

*Department of Electrical and Computer Engineering, University of Massachusetts, Amherst, MA 01003, USA, kestyn@ecs.umass.edu.

†Department of Electrical and Computer Engineering, Department of Mathematics and Statistics, University of Massachusetts, Amherst, MA 01003 USA, polizzi@ecs.umass.edu.

‡Intel Corporation, Santa Clara CA 95054 USA, peter.tang@intel.com

0. Start: Select random subspace $Y_{m_0} \equiv \{y_1, y_2, \dots, y_{m_0}\}_{n \times m_0}$ ($n \gg m_0 \geq m$)
1. Repeat until convergence
2. Compute $Q_{m_0} = \rho(B^{-1}A)Y_{m_0}$
3. Orthogonalize Q_{m_0}
4. Compute $A_Q = Q_{m_0}^H A Q_{m_0}$ and $B_Q = Q_{m_0}^H B Q_{m_0}$
5. Solve $A_Q W = B_Q W \Lambda_Q$ with $W^H B_Q W = I_{m_0 \times m_0}$
6. Compute $Y_{m_0} = Q_{m_0} W$
7. Check convergence of Y_{m_0} and $\Lambda_{Q_{m_0}}$ for the m wanted eigenvalues
8. End

Fig. 1: Subspace iteration method with Rayleigh-Ritz projection

Instead, it is combined with filtering using the function ρ which aims at improving the convergence rate (i.e. $|\rho(\lambda_{m_0+1})/\rho(\lambda_i)|_{i=1,\dots,m}$) by increasing the gap between wanted and unwanted eigenvalues. The filtering function can also be expressed using the spectral decomposition of the Hermitian problem while considering the entire B-orthonormal eigensubspace i.e. $X^H B X = I$.

$$(1.1) \quad \rho(B^{-1}A) = X \rho(\Lambda) X^{-1} \equiv X \rho(\Lambda) X^H B.$$

An ideal filter for the interior eigenvalue problem which maps all m wanted eigenvalues to one and all unwanted ones to zero, can be derived from the Cauchy (or Dunford) integral formula:

$$(1.2) \quad \rho(\lambda) = \frac{1}{2\pi i} \oint_{\mathcal{C}} dz (z - \lambda)^{-1},$$

where the wanted eigenvalues are located inside a complex contour \mathcal{C} . The filter then becomes a spectral projector, with $\rho(B^{-1}A) = X_m X_m^H B$, for the eigenvector subspace X_m (i.e. $\rho(B^{-1}A)X_m = X_m$) and can be written as:

$$(1.3) \quad \rho(B^{-1}A) = \frac{1}{2\pi i} \oint_{\mathcal{C}} dz (zB - A)^{-1} B.$$

The FEAST method proposed in [38, 29], uses a numerical quadrature to approximately compute the action of this filter onto a set of m_0 vectors along the subspace iterations. The resulting rational function ρ_a that approximates the filter (1.2) is given by:

$$(1.4) \quad \rho_a(z) = \sum_{j=1}^{n_e} \frac{\omega_j}{z_j - z},$$

where $\{z_j, \omega_j\}_{1 \leq j \leq n_e}$ are the nodes and related weights of the quadrature. We obtain for the subspace Q_{m_0} in step 2 of the algorithm in Figure 1:

$$(1.5) \quad Q_{m_0} = \rho_a(B^{-1}A)Y_{m_0} = \sum_{j=1}^{n_e} \omega_j (z_j B - A)^{-1} B Y_{m_0} \equiv X \rho_a(\Lambda) X^H B Y_{m_0}.$$

In practice, Q_{m_0} can be computed by solving a small number of (independent) shifted linear systems over a complex contour.

$$(1.6) \quad Q_{m_0} = \sum_{j=1}^{n_e} \omega_j Q_{m_0}^{(j)}, \quad \text{with } Q_{m_0}^{(j)} \text{ solution of } (z_j B - A)Q_{m_0}^{(j)} = B Y_{m_0}$$

The original FEAST paper [29] demonstrated the effectiveness of the approach without analysis of convergence or numerical issues. A detailed numerical analysis on FEAST was completed recently in [38], placing the algorithm on a more solid theoretical foundation. In particular, a relatively small number of quadrature nodes (using Gauss, Trapezoidal or Zolotarev [16] rules) on a circular contour suffices to produce a rapid decay of the function ρ_a from ≈ 1 within the search contour to ≈ 0 outside. In comparison with more standard polynomial filtering [35, 32], the rational filter (1.4) can lead to a very fast convergence of the subspace iteration procedure. In addition, all the m desired eigenvalues are expected to converge at the same rate (since $\rho_a(\lambda_i) \simeq 1$ if λ_i is located within the search interval). The convergence rate of FEAST does not only depend upon the decay properties of the rational function ρ_a , but also on the size of the search subspace m_0 which must not be chosen smaller than the number of eigenvalues inside the search contour (i.e. $m_0 \geq m$). Users of the FEAST eigensolver are responsible for specifying an interval to search for the eigenvalues and a subspace size m_0 that overestimate the number of the wanted eigenvalues. Once these conditions are satisfied, FEAST offers the following set of appealing features:

- (i) high robustness with well-defined convergence rate $|\rho_a(\lambda_{m_0+1})/\rho_a(\lambda_i)|_{i=1,\dots,m}$;
- (ii) all multiplicities naturally captured;
- (iii) no explicit orthogonalization procedure on long vectors required in practice (i.e., step-3 in Figure 1 is unnecessary as long as B_Q is positive definite). We note in (1.5) that Q_{m_0} is naturally spanned by the eigenvector subspace;
- (iv) reusable subspace capable to generate suitable initial guess when solving a series of eigenvalue problems;
- (v) can exploit natural parallelism at three different levels: search intervals can be treated separately (no overlap) while maintaining orthogonality - linear systems can be solved independently across the quadrature nodes of the complex contour - each complex linear system with m_0 multiple right-hand-sides can be solved in parallel. Consequently, within a parallel environment, the algorithm complexity depends on solving a single linear system using a direct or an iterative method.

By allowing the search contour to be placed at arbitrary locations in the complex plane, the FEAST algorithm can be naturally extended to non-Hermitian problems which produce complex eigenvalues. The algorithm retains most of the properties of Hermitian FEAST including the multi-level parallelism. We note, however, a few theoretical and practical difficulties arising which distinguish the non-Hermitian eigenvalue problems from Hermitian ones, including: (i) the treatment of defective systems using the Schur or Jordan forms; (ii) the notion of bi-orthogonality for dual right and left eigenvector subspaces; (iii) the case of ill-conditioned eigenvalue problems that produce sensitive eigenvalues in finite precision arithmetic; (iv) or the shift-invert strategy that may give rise to ill-conditioned linear systems (e.g. if a FEAST quadrature pole lies near a complex eigenvalue).

The key point at which the non-Hermitian FEAST algorithm differs from the Hermitian one is the use of dual subspaces. Since the left and right eigenvectors do not necessarily lie in the same subspace, two separate projectors must then be calculated in order to recover both sets of vectors. A single sided algorithm where only the right subspace is used to project is also possible [37], but will not return a B -bi-orthogonal subspace of left and right eigenvectors, which can be of interest for many applications. In the following, all quantities associated with the left eigenvectors will be written with a $\hat{\cdot}$ symbol (e.g. \hat{X} , \hat{Y} and \hat{Q}). The non-Hermitian algorithm is

similar to its Hermitian counterpart and follows the same steps outlined in Figure 1. A comparison between the main numerical operations for the two algorithms is briefly outlined in Figure 2. The rest of the article aims at providing all the details of the

<u>Hermitian FEAST</u>	<u>Non-Hermitian FEAST</u>
Solving: $AX_m = BX_m\Lambda_m$ $[\Lambda_m]_{ii} \in [\lambda_{min}, \lambda_{max}]$	Solving: $AX_m = BX_m\Lambda_m$ $[\Lambda_m]_{ii} \in \mathcal{C}$ $A^H \widehat{X}_m = B^H \widehat{X}_m \Lambda_m^*$
Inputs: $A = A^H$, B hpd; $m_0 \geq m$; $\{z_1, \dots, z_{n_e}\}$, $\{w_1, \dots, w_{n_e}\}$	Inputs: A and B general; $m_0 \geq m$; $\{z_1, \dots, z_{n_e}\}$, $\{w_1, \dots, w_{n_e}\}$
$Y_{m_0} \leftarrow m_0$ initial vectors	$Y_{m_0}, \widehat{Y}_{m_0} \leftarrow m_0$ initial vectors;
repeat	repeat
$Q_{m_0} = 0$	$Q_{m_0} = \widehat{Q}_{m_0} = 0$
for $j = 1, n_e$	for $j = 1, n_e$
$Q_{m_0}^{(j)} \leftarrow (z_j B - A)^{-1} B Y_{m_0}$;	$Q_{m_0}^{(j)} \leftarrow (z_j B - A)^{-1} B Y_{m_0}$;
$Q_{m_0} \leftarrow Q_{m_0} + \omega_j Q_{m_0}^{(j)}$	$\widehat{Q}_{m_0}^{(j)} \leftarrow (z_j^* B^H - A^H)^{-1} B^H \widehat{Y}_{m_0}$
end	$Q_{m_0} \leftarrow Q_{m_0} + \omega_j Q_{m_0}^{(j)}$
$B_Q \leftarrow Q_{m_0}^H B Q_{m_0}$	$\widehat{Q}_{m_0} \leftarrow \widehat{Q}_{m_0} + \omega_j^* \widehat{Q}_{m_0}^{(j)}$
Check B_Q hpd (resizing step)	end
$A_Q \leftarrow Q_{m_0}^H A Q_{m_0}$	$B_Q \leftarrow \widehat{Q}_{m_0}^H B Q_{m_0}$
Solve $A_Q W = B_Q W \Lambda_Q$; $W^H B_Q W = I$	Check B_Q non-singular (resizing step)
$Y_{m_0} \leftarrow Q_{m_0} W$	$A_Q \leftarrow \widehat{Q}_{m_0}^H A Q_{m_0}$
until Convergence of Y_m, Λ_{Q_m}	Solve $A_Q \widehat{W} = B_Q \widehat{W} \Lambda_Q$ and
with $[\Lambda_{Q_m}]_{ii} \in [\lambda_{min}, \lambda_{max}]$	$A_Q^H \widehat{W} = B_Q^H \widehat{W} \Lambda_Q^*$; $\widehat{W}^H B_Q W = I$
Output: $X_m \equiv Y_m$ ($X_m^H B X_m = I_m$); $\Lambda_m \equiv \Lambda_{Q_m}$	$Y_{m_0} \leftarrow Q_{m_0} W$, $\widehat{Y}_{m_0} \leftarrow \widehat{Q}_{m_0} \widehat{W}$
	until Convergence of $Y_m, \widehat{Y}_m, \Lambda_{Q_m}$
	with $[\Lambda_{Q_m}]_{ii} \in \mathcal{C}$
	Output: $X_m \equiv Y_m$; $\widehat{X}_m \equiv \widehat{Y}_m$ ($\widehat{X}_m^H B X_m = I_m$); $\Lambda_m \equiv \Lambda_{Q_m}$

Fig. 2: Brief outlook and comparison between the main numerical operations for the FEAST algorithms applied to the Hermitian and non-Hermitian problems.

non-Hermitian FEAST algorithm and its practical implementation. Section 2 presents multiples theoretical and practical algorithmic considerations, outlines the differences with the Hermitian FEAST algorithm, and ends with a complete description of the non-Hermitian algorithm with discussions on limitations. Section 3 briefly outlines some features of the new FEAST eigensolver version 3.0, from which the proposed changes here take effect. We conclude by presenting some numerical experiments in Section 4.

2. Theoretical and Practical Considerations.

2.1. Defining a search contour. A key feature of FEAST is the ability to calculate a subset of eigenvalues that exist within some interval. Figure 3 summarizes the different search contour options possible for both the Hermitian and non-Hermitian FEAST algorithms.

For the Hermitian case, the user must then specify a 1-dimensional real-valued search interval $[\lambda_{min}, \lambda_{max}]$. These two points are used to define a circular or ellipsoid contour \mathcal{C} centered on the real axis, and along which the complex integration nodes

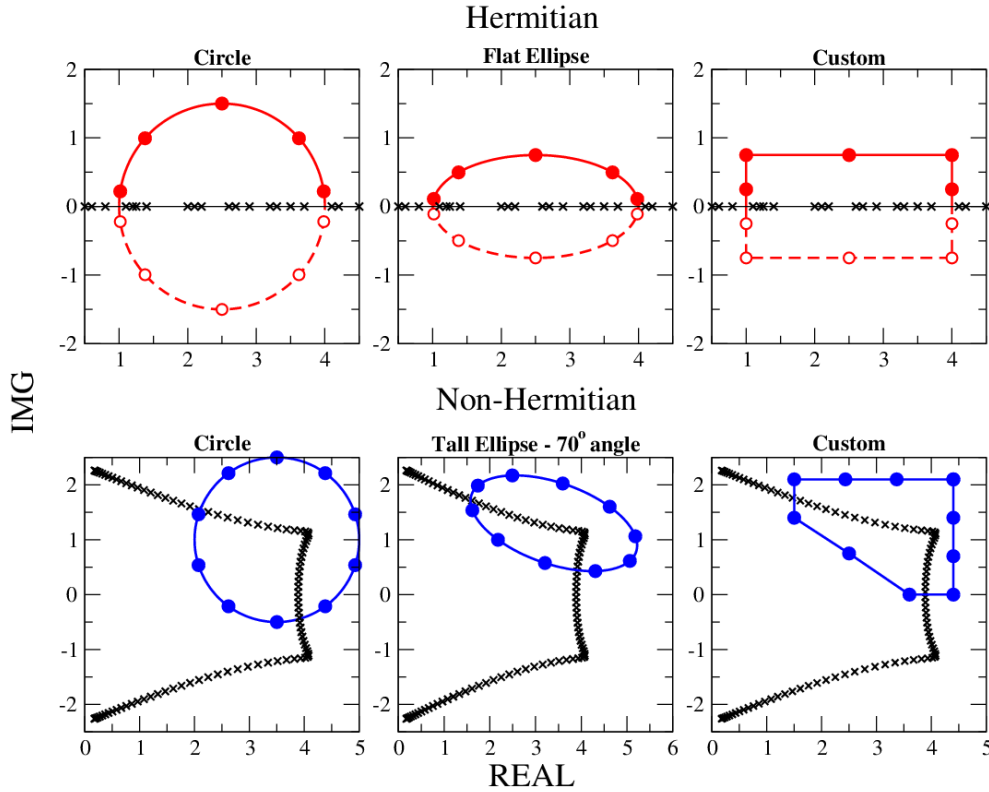


Fig. 3: Various search contour examples for the Hermitian and the non-Hermitian FEAST algorithms. Both algorithms feature standard ellipsoid contour options and the possibility to define custom arbitrary shapes. In the Hermitian case, the contour is symmetric with the real axis and only the nodes in the upper-half may be generated. In the non-Hermitian case, a full contour is needed to enclose the wanted complex eigenvalues.

are generated. The choice of a particular quadrature rule will lead to a different set of relative positions for the nodes and associated quadrature weights i.e. $\{z_j, \omega_j\}$. Since the eigenvalues are real, it is convenient to select a symmetric contour with the real axis (i.e. $\mathcal{C} = \mathcal{C}^*$) since it only requires one to operate the quadrature on the half-contour (e.g. upper half).

With a non-Hermitian problem, it is necessary to specify a 2-dimensional search contour that surrounds the wanted complex eigenvalues. Circular or ellipsoid contours can also be used and they can be generated using standard options included into FEAST v3.0. These are defined by a complex midpoint λ_{mid} and a radius r for a circle (for an ellipse the ratio between the horizontal axis and vertical axis diameter can also be specified, as well as an angle of rotation). However, in some applications where the eigenvalues of interest belong to a particular subset in the complex plane, more flexibility for selecting a search contour with arbitrary shape could be needed. This option also lends itself to parallelism, where a large number of eigenvalues can be calculated by partitioning the complex plane into multiple contours (see Section

4). Consequently, a ‘‘Custom Contour’’ feature is also supported in FEAST v3.0 that allows to account for arbitrary quadrature nodes and weights.

2.2. Right/Left Spectral Projectors and Dual Subspaces. The filtering function can be applied to any similarity transformation of the pencil, the most general of which is the Jordan Normal Form.

$$(2.1) \quad \rho(B^{-1}A) = X\rho(J)X^{-1}.$$

When applied to each Jordan block J_k , the expression of the operator becomes [19]:

$$(2.2) \quad \rho(J_k) = \rho \left(\begin{bmatrix} \lambda_k & 1 & \dots & 0 \\ 0 & \lambda_k & \ddots & \vdots \\ \vdots & \ddots & \ddots & 1 \\ 0 & \dots & 0 & \lambda_k \end{bmatrix} \right) = \begin{bmatrix} \rho(\lambda_k) & \frac{\rho'(\lambda_k)}{0!} & \dots & \frac{\rho^{(m)}(\lambda_k)}{(m-1)!} \\ 0 & \rho(\lambda_k) & \ddots & \vdots \\ \vdots & \ddots & \ddots & \frac{\rho'(\lambda_k)}{0!} \\ 0 & \dots & 0 & \rho(\lambda_k) \end{bmatrix}$$

Using the Cauchy integral formula (1.2), the diagonal elements of J_k take the values one or zero, while all derivatives (i.e. off-diagonal elements) are zero. In practice, this may not be guarantee with FEAST as the filter is approximated by the rational function (1.4). A generalization of the algorithm for addressing the defective systems would require further studies, and our current FEAST non-Hermitian algorithm assumes that the Jordan form reduces to an eigenvalue decomposition. Consequently, we consider:

$$(2.3) \quad \rho(B^{-1}A) = X\rho(\Lambda)X^{-1} \equiv X\rho(\Lambda)\widehat{X}^H B,$$

where the left and right eigensubspaces satisfy the B -bi-orthonormal relationship i.e. $\widehat{X}^H B X = I$. For the case of the Hermitian problem, we note that $\widehat{X} = X$ and the relation (1.1) can then be recovered. It is also important to mention the particular case of complex symmetric systems (i.e. $A = A^T$ and $B = B^T$) which leads to $\widehat{X} = X^*$. In general, however, the left and right vectors are not straightforwardly related and they must be calculated explicitly.

From (1.2), (1.3), and (2.3), one can define the right spectral projector $\rho(B^{-1}A)$ for the right eigenvector subspace X_m (i.e. $\rho(B^{-1}A)X_m = X_m$) as follow:

$$(2.4) \quad \rho(B^{-1}A) = \frac{1}{2\pi i} \oint_{\mathcal{C}} dz (zB - A)^{-1} B \equiv X_m \widehat{X}_m^H B.$$

For the treatment of the left eigenvector subspace solution of $\widehat{X}^H A = \Lambda \widehat{X}^H B$, it is first convenient to define the following eigenvalue decomposition:

$$(2.5) \quad \rho(AB^{-1}) = \widehat{X}^{-H} \rho(\Lambda) \widehat{X}^H \equiv B X \rho(\Lambda) \widehat{X}^H.$$

One can then construct the left spectral projector $\rho(AB^{-1})$ (i.e. $\widehat{X}_m^H = \widehat{X}_m^H \rho(AB^{-1})$) as:

$$(2.6) \quad \rho(AB^{-1}) = \frac{1}{2\pi i} \oint_{\mathcal{C}} dz B (zB - A)^{-1} \equiv B X_m \widehat{X}_m^H.$$

In FEAST, the projectors are formulated using the rational function ρ_a (1.4) along with the quadrature nodes and weights $\{z_j, \omega_j\}_{1 \leq j \leq n_e}$ that approximate the contour integrations in (2.4) and (2.6). The right and left subspaces Q_{m_0} and \widehat{Q}_{m_0} are then obtained by applying the right and left projectors onto a set of m_0 vectors i.e.

$$(2.7) \quad Q_{m_0} = \rho_a(B^{-1}A)Y_{m_0} = \sum_{j=1}^{n_e} \omega_j (z_j B - A)^{-1} B Y_{m_0} \equiv X \rho_a(\Lambda) \widehat{X}^H B Y_{m_0}.$$

and

$$(2.8) \quad \widehat{Q}_{m_0}^H = \widehat{Y}_{m_0}^H \rho_a(AB^{-1}) = \sum_{j=1}^{n_e} \omega_j \widehat{Y}_{m_0}^H B (z_j B - A)^{-1} \equiv \widehat{Y}_{m_0}^H B X \rho_a(\Lambda) \widehat{X}^H.$$

In practice, the calculation of both subspaces require solving a series of linear systems. For the right subspace,

$$(2.9) \quad Q_{m_0} = \sum_{j=1}^{n_e} \omega_j Q_{m_0}^{(j)}, \quad \text{with } Q_{m_0}^{(j)} \text{ solution of } (z_j B - A) Q_{m_0}^{(j)} = B Y_{m_0},$$

which was already outlined in (1.6), and for the left subspace:

$$(2.10) \quad \widehat{Q}_{m_0} = \sum_{j=1}^{n_e} \omega_j^* \widehat{Q}_{m_0}^{(j)}, \quad \text{with } \widehat{Q}_{m_0}^{(j)} \text{ solution of } (z_j B - A)^H \widehat{Q}_{m_0}^{(j)} = B^H \widehat{Y}_{m_0}.$$

These numerical operations are also described in Figure 2. As a result of (2.7) and (2.8), Q_{m_0} (resp. \widehat{Q}_{m_0}) is formed by a linear combinations of the columns of X_{m_0} (resp. \widehat{X}_{m_0}). The Rayleigh-Ritz procedure should then involve the reduced matrices A_Q and B_Q formed by projecting on the right with a subspace containing the right eigenvectors Q_{m_0} , and projecting on the left with a subspace containing the left eigenvectors \widehat{Q}_{m_0} . The resulting non-Hermitian reduced system can be solved using the QZ algorithm [27] in LAPACK [1] to yield the right and left eigenvectors W and \widehat{W} defined in Figure 2. The long right (resp. left) Ritz vectors can then be recovered as $Y_{m_0} = Q_{m_0} W$ (resp. $\widehat{Y}_{m_0} = \widehat{Q}_{m_0} \widehat{W}$), and used as initial guess subspaces for the next FEAST iterations until convergence.

2.3. Discussions on Convergence. In our implementation of FEAST, the criteria of convergence is satisfied if the norm of the relative residual associated with the eigenpairs (x_i, λ_i) and $(\widehat{x}_i, \lambda_i^*)$, is found below an arbitrary threshold ϵ i.e.

$$(2.11) \quad res_i = \max \left\{ \frac{\|Ax_i - \lambda_i Bx_i\|_1}{\|\alpha Bx_i\|_1}, \frac{\|A^H \widehat{x}_i - \lambda_i^* B^H \widehat{x}_i\|_1}{\|\alpha B^H \widehat{x}_i\|_1} \right\} < \epsilon,$$

where the value of ϵ can be chosen typically equal to 10^{-13} if high accuracy is needed using double precision arithmetic. The parameter α is relative to the eigenvalue range in the search contour. The latter is defined differently for the Hermitian and non-Hermitian cases (as discussed in Section 2.1), and a non-zero value for α can be chosen as $\alpha = \max(|\lambda_{min}|, |\lambda_{max}|)$ for the Hermitian case and $\alpha = (|\lambda_{mid}| + r)$ for the non-Hermitian case.

As discussed in the introduction section, the right/left eigenvectors associated with λ_i with $i = 1, \dots, m$ (and hence all associated residuals res_i) are expected to

converge linearly along the FEAST subspace iterations at the rate: $|\rho_a(\lambda_{m_0+1})/\rho_a(\lambda_i)|$ for $i = 1, \dots, m$. The convergence depends then on both the subspace size m_0 ($m_0 \geq m$) and the accuracy of the rational filter ρ_a (1.4) that should ideally provide values very close to unity for eigenvalues on the interior of the search contour and zero elsewhere. Although quite effective, the Gauss-quadrature approach along a circular contour that was proposed in the original FEAST article [29], is clearly not the only possible choice for optimizing the convergence ratio. Three other options have already been considered for the Hermitian problem including [16]: (i) the Trapezoidal rule; (ii) different contour shapes beside a circle such as a finely tuned flat ellipse; (iii) a new approximation of the spectral projector based on a Zolotarev approximant to the sign function which, after transformations, provides complex poles on the unit circle [42, 16]. Both Gauss and Zolotarev are well-suited choices for the Hermitian problem since they favor an accentuation of the decay of $|\rho_a|$ at the boundaries of the interval along the real axis. The Trapezoidal rule, in turn, leads to a more uniform decay for $|\rho_a|$ in any directions of the complex plane [37], and it is also well-known for its exponential convergence property with the number of integration nodes n_e [40]. The Trapezoidal rule is then expected to provide more consistency for capturing the complex eigenvalues of the non-Hermitian problem.

Similarly to the Hermitian problem, the non-Hermitian FEAST algorithm also requires as input a search subspace of size m_0 chosen not smaller than the number of eigenvalues m within a given complex contour. If m_0 ($m_0 \geq m$) is chosen too small, the ratio governing the convergence may come closer to one, leading to slow convergence. Alternatively, if m_0 is chosen too large, it may result in an unnecessary high number of right-hand-sides when solving the shifted linear systems in (2.9) and (2.10). Two examples have been designed to illustrate the convergence rates dependence on m_0 . These tests use the QC324 matrix from the NEP collection [2]. A contour has been created with a single eigenvalue λ_1 inside. The contour and few closest eigenvalues can be seen in Figure 4. The rational function $|\rho_a|$ which has been generated using a six-point Trapezoidal rule is also shown in the figure (as a contour plot on the left and a 3-D surface plot on the right). Figure 5 shows the convergence of the relative residual norms for all the m_0 eigenvalues along the FEAST subspace iterations in the cases $m_0 = 2$ (left plot) and $m_0 = 4$ (right plot). For $m_0 = 2$, λ_3 is the closest eigenvalue outside of the search subspace and controls the convergence rate. Since this eigenvalue is relatively close to the contour, FEAST exhibits slow convergence. The case $m_0 = 4$, in turn, leads to drastic improvement in the convergence rate which benefits from the small values of $\rho_a(\lambda_5)$.

A typical recommended choice for the search subspace size is $m_o = 2m$. In practice, however, the exact number of eigenvalues m is unknown beforehand and the user must make an educated guess. Alternatively, m can also be estimated using, for example, the fast stochastic estimate procedure [8] that has been recently introduced in FEAST v3.0. It is important to note that in some situations slow convergence can result if the value of m_0 is only large enough to include the external eigenvalues bordering the contour. This problem can arise when the eigenvalues of interest are near a continuum or cluster of eigenvalues. With many eigenvalues closely bordering the contour, it may not be possible to improve convergence by increasing the subspace size m_0 . In this case, using additional integration nodes to increase the accuracy of ρ_a may be necessary. A utility routine for calculating the rational function has also been included in FEAST v3.0 and can be used to investigate convergence for different contours and eigenvalue distributions.

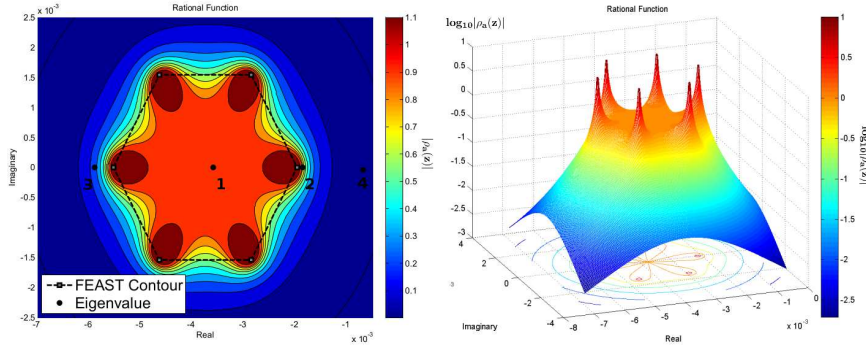


Fig. 4: Value of the rational function plotted as contour plot (left) and surface plot (right) using a hexagonal contour for the QC324 matrix. The left plot includes the positions of the four closest eigenvalues. Only a single eigenvalue λ_1 is inside of the contour. More particularly, we note that $|\rho_a(\lambda_1)| = 1.0000004$, $|\rho_a(\lambda_2)| = 1.7272309$, $|\rho_a(\lambda_3)| = 0.4206553$, $|\rho_a(\lambda_4)| = 3.6296209 \times 10^{-2}$, and $|\rho_a(\lambda_5)| = 6.9332547 \times 10^{-3}$. The latter is associated with the eigenvalue λ_5 which cannot be seen in the Figure since it is out of range.

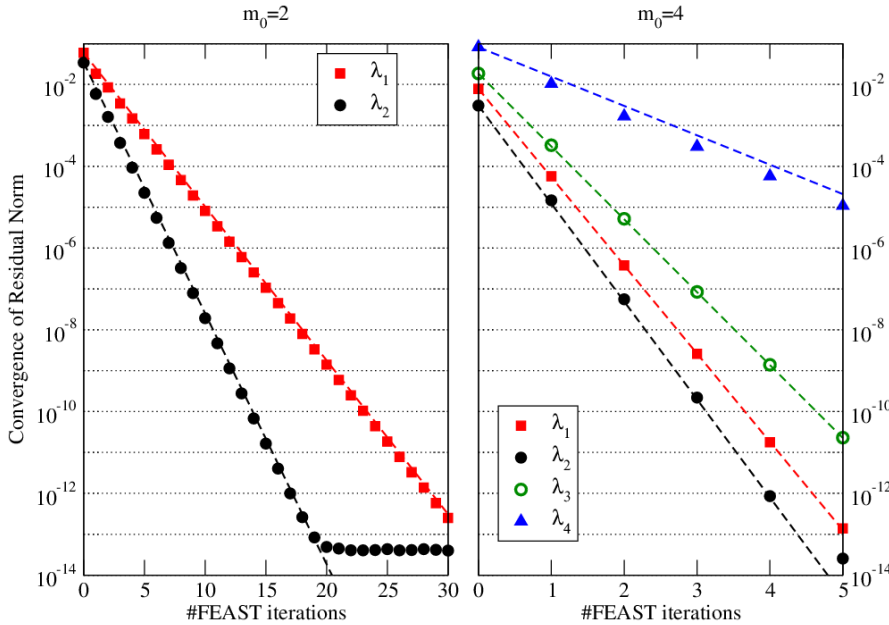


Fig. 5: Convergence of the residual norms (2.11) associated with eigenvalues λ_i in Figure 4. Two search subspace size are considered $m_0 = 2$ (left plot) and $m_0 = 4$ (right plot). The dashed lines represent the theoretical linear convergence rate $|\rho_a(\lambda_{m_0+1})/\rho_a(\lambda_i)|$ which is perfectly matched by the values returned by FEAST. We note that the convergence of the wanted eigenvalue λ_1 is considerably slower using the smaller size subspace $m_0 = 2$ since the eigenvalue λ_3 , that governs the convergence rate for this case, ends up being too close to the search contour.

Finally, and in contrast to the Hermitian problem where the contour nodes can be placed away from the eigenvalues (i.e. far enough from the real axis), a contour node could end up being located in the vicinity of a complex eigenvalue. In this case the rational function could take on values larger than one, and it becomes then possible for an eigenvalue outside of the contour to converge at a faster rate than the wanted eigenvalues inside. This is what is happening to λ_2 in Figures 4 and 5. If a contour node is located too close to an eigenvalue, however, it is likely to worsen the conditioning of the corresponding shifted linear system in (2.9) and (2.10), making then the problem more challenging to solve using an iterative method.

2.4. Reduced Contour Integration Cost. Non-Hermitian matrices A and B come in three flavors: (i) complex general, (ii) real non-symmetric, and (iii) complex symmetric. The major computational task performed by FEAST is the numerical integration, where a set of linear systems must be solved along a complex contour. In the complex general case both Q_{m_0} and \widehat{Q}_{m_0} are computed explicitly by solving the $2n_e$ (independent) linear systems defined in (2.9) and (2.10). It is important to note that most modern numerical libraries that includes direct methods for solving linear systems, supply a “transpose conjugate solve” feature as well (i.e. a linear system $A^H x = f$ can be solved using the factorization of A). Consequently, once the $(z_j B - A)$ matrices are factorized in (2.9), the system solves in (2.10) can be performed without re-factorizing the conjugate transpose of the matrices. Similarly using iterative methods, the conjugate transpose solve could be performed without factorizing twice the preconditioner. If such option is available, the contour integration in the most general case should involve only n_e (independent) factorizations and $2n_e$ (independent) solves with m_0 right hand sides. For the cases (ii) and (iii) above, it is possible to take advantage of some additional matrix properties that result in a reduced workload as discussed in following.

Complex symmetric - For the complex symmetric case ($A = A^T$ and $B = B^T$), there exists a relationship between the left and right eigenvectors, which can be expressed as conjugate pairs i.e. $\widehat{X} = X^*$. This allows the left subspace \widehat{Q} to be expressed in terms of the right Q using the same simple relationship $\widehat{Q} = Q^*$. Therefore \widehat{Q} (2.10) does not need to be calculated, and only the n_e factorizations and n_e solves in (2.9) are then necessary.

Real non-symmetric - In general the treatment of the real non-symmetric case ($A = A^*$ and $B = B^*$) is identical to the complex non-symmetric one. However, there exists some savings for specific contours exhibiting symmetry across the real axis (i.e $\mathcal{C} = \mathcal{C}^*$). For this particular case, each integration node z_j with $j = 1, \dots, n_e/2$ in the upper half of the complex plane has a conjugate pair z_j^* in the lower half. From the resulting following relationships:

$$(z_j B - A)^* = (z_j^* B - A) \quad \text{and} \quad (z_j B - A)^H = (z_j^* B - A)^T,$$

one can show that only the $n_e/2$ factorizations of $(z_j B - A)$ in the upper-half contour, along with n_e total solves, are needed to obtain both Q_{m_0} and \widehat{Q}_{m_0} in (2.9) and (2.10).

The contour integration cost can then be reduced depending on the properties of the eigenvalue system, attributes of the complex contour (e.g. if $\mathcal{C} = \mathcal{C}^*$), or the standard feature of transpose conjugate solve offered by most linear system solvers.

Table 1 summarizes the number of factorizations and solves effectively needed to perform the full contour integration using a total of n_e nodes. The cost of the Hermitian FEAST algorithm is also provided for reference.

Family of eigenvalue problems	(A,B) properties	#Factorizations	#Solves
Complex general	N/A	n_e	$2n_e$
Complex symmetric	$A = A^T, B = B^T$	n_e	n_e
Complex Hermitian with $\mathcal{C} = \mathcal{C}^*$	$A = A^H, B$ hpd	$n_e/2$	n_e
Real non-symmetric	N/A	n_e	$2n_e$
Real non-symmetric with $\mathcal{C} = \mathcal{C}^*$	N/A	$n_e/2$	n_e
Real symmetric with $\mathcal{C} = \mathcal{C}^*$	$A = A^T, B$ spd	$n_e/2$	$n_e/2$

Table 1: Summary of the total number of factorizations and solves effectively needed by FEAST to perform the full contour integration using a total of n_e nodes. It is also assumed that the transpose conjugate solve feature is available for the system solver.

2.5. Resizing the search subspace. The rank of the subspaces Q_{m_0} (2.7) and \widehat{Q}_{m_0} (2.8) is greater than or equal to the number of wanted eigenvalues m ($m_0 \geq m$) since the eigenpairs outside of the contour are also accounted for due to inaccuracies in the numerical integration. In turn, if m_0 is too severely overestimated the rank may end up being less than the subspace size m_0 in finite precision arithmetic. Consequently, m_0 must then be resized to prevent the subspaces to become numerically rank deficient and the reduced matrix $B_Q = \widehat{Q}_{m_0}^H B Q_{m_0}$ singular. Otherwise, the QZ algorithm used in the computation of the reduced system can produce infinite eigenvalue solutions [27]. Re-injecting these solutions into the subspace iteration would cause problems for the algorithm. The upper bound for the choice of m_0 should be the largest value before the subspaces become numerically rank deficient. One possible way to determine this threshold value consists of performing the spectral decomposition of B_Q and analyzing its eigenvalues. It comes:

$$(2.12) \quad B_Q = V\Gamma\widehat{V}^H,$$

where Γ is the diagonal matrix for the eigenvalues $\{\gamma_i\}_{i=1,\dots,m_0}$, and V and \widehat{V} are respectively the corresponding left and right bi-orthonormal eigenvector subspaces (i.e. $\widehat{V}^H V = I_{m_0}$). We note that for the Hermitian case where B and hence B_Q must be positive definite, this step is replaced by monitoring the failure of the Cholesky factorization of B_Q that could return a negative pivot. The position of the latter helped determining the threshold value for m_0 used to resize the subspace accordingly. For the non-Hermitian problem, the matrix B_Q is singular if there exists an eigenvalue equal to zero. In finite precision arithmetic, a zero eigenvalue must be characterized relatively i.e.

$$(2.13) \quad |\gamma_i| < \eta * \max \{|\gamma_1|, \dots, |\gamma_{m_0}|\},$$

where η is relative to the machine precision; e.g. 10^{-16} in double precision. If an eigenvalue γ_i is then different than the maximum eigenvalue by 16 orders-of-magnitude then it is out of range for the double precision arithmetic and is counted as a zero. The subspace m_0 is resized to \tilde{m}_0 such that B_Q has no eigenvalues satisfying (2.13). The spectral decomposition of B_Q is computed at each FEAST iteration, and as it

will be discussed in the next section, the resizing is performed in conjunction with a B -bi-orthonormalization for the subspaces $Q_{\tilde{m}_0}$ and $\widehat{Q}_{\tilde{m}_0}$. The additional numerical cost of diagonalizing B_Q is on the order of (but less expensive than) the cost associated with the diagonalization of the reduced generalized system.

As a side remark, it is interesting to note that using the expression (2.7) and (2.8), B_Q can also be written as:

$$(2.14) \quad B_Q = (\widehat{Y}_{m_0}^H B X) \rho_a^2(\Lambda) (\widehat{X}^H B Y_{m_0}).$$

Starting from the second FEAST iteration where the Ritz vectors Y_{m_0} and \widehat{Y}_{m_0} are not only span respectively by the true eigenvector subspaces X and \widehat{X} but they also satisfy the property of B -bi-orthonormality (i.e. $\widehat{Y}_{m_0}^H B Y_{m_0} = I$ since $\widehat{W}^H B_Q W = I$ in Figure 2), it is possible to directly identify (2.14) with (2.12). It comes that $V = \widehat{Y}_{m_0}^H B X$, $\widehat{V}^H = \widehat{X}^H B Y_{m_0}$, and $\Gamma = \rho_a^2(\Lambda)$. The latter indicates that the eigenvalues of B_Q are related to the rational function ρ_a , and can then be used to estimate the convergence rate [38]. In order for $|\rho_a|$ to satisfy (2.13), however, η should be replaced by $\sqrt{\eta}$. Consequently, the convergence rate for the algorithm is here limited to 10^{-8} in double precision arithmetic (a similar argument could be made for the case of the Hermitian FEAST which relies on the Cholesky decomposition of the normal-type equation B_Q). FEAST can then converge in a minimum of 2 iterations to machine precision at $\sim 10^{-16}$ given a sufficiently large enough subspace size m_0 (whose value is also relative to the accuracy of ρ_a). If needed, it may be possible to obtain higher convergence rate (i.e one FEAST iteration) using a direct robust QR factorization or singular value decomposition (SVD) of the subspaces Q_{m_0} and \widehat{Q}_{m_0} .

2.6. B-bi-orthonormalization. The intended result of FEAST is a set of B -bi-orthonormal vectors. However, the B -bi-orthogonality is not guaranteed after the contour integration due to numerical inaccuracies. This is especially pronounced in large problems which exhibit a continuum of eigenvalues bordering the search contour. The contour integration could potentially include a large number of mixed states from the continuum in the subspaces Q_{m_0} (2.7) and \widehat{Q}_{m_0} (2.8). In our numerical experiments, we have found that an explicit B -bi-orthonormalization of the FEAST subspaces Q_{m_0} and \widehat{Q}_{m_0} helps improving the stability of the algorithm. Rather than performing a QR factorization or SVD of the subspaces, we aim at taking advantage of the eigen-decomposition of B_Q (2.12) that is already performed in FEAST as discussed in the previous section. From (2.12) and since $B_Q = \widehat{Q}_{m_0}^H B Q_{m_0}$, it comes:

$$(2.15) \quad \Gamma = \widehat{V}^H B_Q V = (\widehat{V}^H \widehat{Q}_{m_0}^H) B (Q_{m_0} V) \equiv (\widehat{Q}_{m_0} \widehat{V})^H B (Q_{m_0} V).$$

As a result, B -bi-orthonormal subspaces U_{m_0} and \widehat{U}_{m_0} can be generated by updating the current subspaces Q_{m_0} and \widehat{Q}_{m_0} as follows:

$$(2.16) \quad U_{m_0} = Q_{m_0} V \Gamma^{-1/2}, \quad \widehat{U}_{m_0} = \widehat{Q}_{m_0} \widehat{V} \Gamma^{-H/2}.$$

As discussed in the previous section, the subspace size m_0 may have already been reduced to \tilde{m}_0 at this stage by allowing the eigenvectors in V and \widehat{V} , corresponding to the zero eigenvalues in Γ , to be removed from the subspace. In practice, a subset of V and \widehat{V} composed of \tilde{m}_0 columns vectors can be easily extracted if the eigenpairs $\{\gamma_i, v_i \equiv V e_i, \widehat{v}_i \equiv \widehat{V} e_i\}_{i=1, \dots, m_0}$ are first sorted by decreasing values of $|\gamma_i|$. Denoting $V_{m_0 \times \tilde{m}_0}$ and $\widehat{V}_{m_0 \times \tilde{m}_0}$ the subsets of the new V and \widehat{V} subspaces restricted to their

first \tilde{m}_0 columns, and $\Gamma_{\tilde{m}_0 \times \tilde{m}_0}$ the matrix of the first \tilde{m}_0 sorted eigenvalues, (2.16) becomes:

$$(2.17) \quad U_{\tilde{m}_0} = Q_{m_0} V_{m_0 \times \tilde{m}_0} \Gamma_{\tilde{m}_0 \times \tilde{m}_0}^{-1/2}, \quad \hat{U}_{\tilde{m}_0} = \hat{Q}_{m_0} \hat{V}_{m_0 \times \tilde{m}_0} \Gamma_{\tilde{m}_0 \times \tilde{m}_0}^{-H/2}.$$

Thereafter, the matrices of the reduced system can be obtained using a new Rayleigh-Ritz projection for A and B i.e. $B_U = \hat{U}_{\tilde{m}_0}^H B U_{\tilde{m}_0}$ and $A_U = \hat{U}_{\tilde{m}_0}^H A U_{\tilde{m}_0}$. In spite of our B -bi-orthonormalization procedure, the resulting B_U is not necessarily identity, or even diagonal, due to numerical inaccuracies and finite precision arithmetic. However, this procedure is beneficial as a precursor to the QZ algorithm used to solve the reduced generalized problem, since it helps to remove contaminating eigenvalues that lie close to the contour. The benefits of our B -bi-orthonormalization step can be seen in Figure 6. This test has been run on the CSH4 matrix [7], an 801×801 complex scaled Hamiltonian from the BigDFT electronic structure code [14]. The eigenspectrum and the desired eigenvalues inside of a FEAST custom contour can be seen on the left side of Figure 6. One edge of the contour is parallel to the eigenvalue continuum. This results in a large number of mixed states after spectral projections in (2.7) and (2.8). Without bi-orthonormalization, the QZ algorithm fails to return a B -bi-orthogonal set of eigenvectors for large values of m_0 . The minimum obtained convergence then degrades for larger subspace sizes. By employing our bi-orthogonalization procedure the QZ algorithm is more stable and is able to return a B -bi-orthogonal set. The minimum obtained convergence remains constant for all m_0 values as shown in Figure 6 (right plot). Note that the B_Q matrix remains non-singular for all values of m_0 and no resizing operations have then been performed (i.e. $B_U \equiv B_Q$).

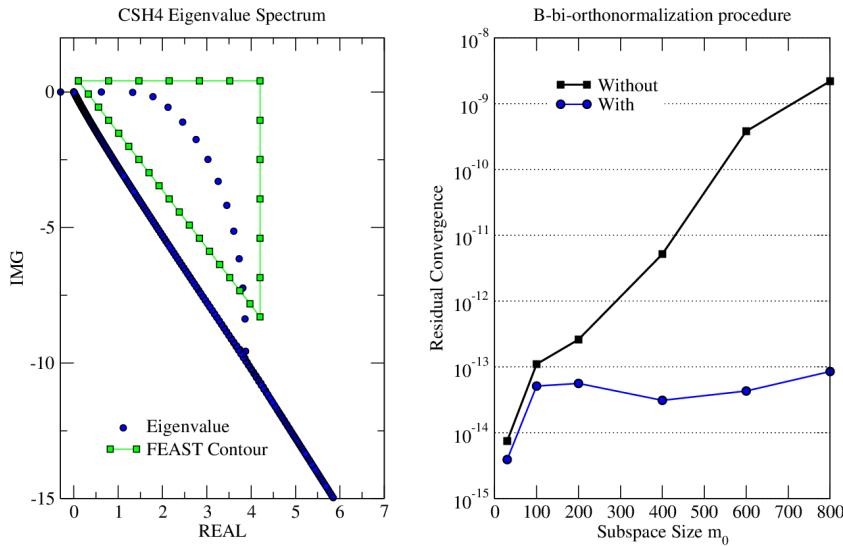


Fig. 6: On the left: eigenvalue spectrum of CSH4. On the right: minimum obtained convergence of the residual norm (2.11) after 20 FEAST iterations plotted in function of the subspace size m_0 . With our bi-orthonormalization procedure, the minimum obtained convergence stays relatively constant for all m_0 .

2.7. Spurious Solutions. In certain situation incorrect eigenvalues, so called spurious solutions, appear inside of the FEAST contour. These spurious eigenvalues do not converge. It is important to note that the corresponding spurious eigenvectors do not need to be explicitly removed from the search subspace to guarantee that the true solutions will converge along the FEAST iterations. Spurious solutions could then be flagged a posteriori once FEAST has converged. The spurious problem, however, leads to the practical issue of devising a suitable convergence test.

In FEAST v2.1 for the Hermitian case using Gauss quadrature along a circle contour, the true number of eigenvalues m could be obtained by counting the eigenvalue of B_Q (see (2.12) using $\widehat{V} = V$) satisfying the condition $|\gamma_i| \leq 1/4$ [38, 12] (i.e. $|\rho_a(\lambda_i)| \leq 1/2$ from (2.14)) which guaranteed that λ_i is a true eigenvalue within $[\lambda_{min}, \lambda_{max}]$. Since FEAST v3.0 is allowing for custom contour in the complex plane, it is not possible to perform a similar test by simply analyzing the values $|\gamma_i|$. A new strategy has been developed, which can be used to provide increasingly better estimate of the number of true eigenvalue solutions in the search subspace at each the FEAST subsequent iteration.

By definition, if a Ritz eigenpair $(\lambda_i, y_i, \widehat{y}_i)$ obtained after solving the reduced system is a genuine solution of the matrix pencil (A,B), then the eigenpair $(\rho(\lambda_i), y_i, \widehat{y}_i)$ is also a solution for $\rho(B^{-1}A)$ (2.3) and $\rho(AB^{-1})$ (2.5). In practice, one can perform a comparison between a direct calculation of $\rho(\lambda_i)$ where λ_i is the Ritz value, and the value $\rho(\lambda_i)$ solution of $\rho(B^{-1}A)y_i \simeq \rho(\lambda_i)y_i$ (which is only approximated if the Ritz vectors have not yet converged). A suitable choice for the function ρ should allow these two values for $\rho(\lambda_i)$ to differ significantly if λ_i is spurious, with the condition that $\widehat{y}_i^H B \rho(B^{-1}A)y_i \simeq \rho(\lambda_i)$ can also be easily calculated. The choice of the approximate spectral projector ρ_a^2 (1.4) satisfy both conditions. Using (2.7) and (2.14), we note that:

$$(2.18) \quad \rho_a^2(\lambda_i) \simeq \widehat{y}_i^H B \rho_a^2(B^{-1}A)y_i = \widehat{y}_i^H B X \rho_a^2(\Lambda) \widehat{X}^H B y_i \equiv [B_Q]_{i,i},$$

where $[B_Q]_{ii}$ denotes the i^{th} diagonal element of B_Q . Our identification procedure for the spurious solutions can then be summarized by the following three steps:

1. Compute the corresponding $\{\rho_a(\lambda_i)\}_{i=1,\dots,m_0}$ using (1.4) and the Ritz values solution of the reduced system $\{\lambda_i\}_{i=1,\dots,m_0}$; i.e.

$$(2.19) \quad \rho_a(\lambda_i) = \sum_{j=1}^{n_e} \frac{\omega_j}{z_j - \lambda_i},$$

2. Form the Ritz vectors and wait for the contour integration to be performed and B_Q constructed at the next FEAST iteration.
3. Compare the calculated values of $\rho_a(\lambda_i)$ with the corresponding diagonal values of $[B_Q]_{ii}$ (which are already sorted), and label λ_i as spurious if it satisfies the following inequality:

$$(2.20) \quad \left| \frac{\rho_a^2(\lambda_i) - [B]_{ii}}{\rho_a^2(\lambda_i)} \right| \geq \mu,$$

where μ is empirically chosen to be 10^{-1} . We have found that this criteria is both large enough to flag all the spurious solutions, and small enough to ensure that true solutions are not mislabeled as soon as they start converging.

Once a Ritz eigenpair is flagged as spurious, it is kept in the search subspace but it is not accounted for in the test for the residual convergence (2.11). On exit, however, a sorting procedure on the subspace is used by FEAST to return the converged eigenpairs free from spurious solutions.

2.8. Summary and Complete Algorithm. The algorithm in Figure 7 provides a complete description of non-Hermitian FEAST. The algorithm presents six stages from initialization to convergence test, that further detail the different numerical operations outlined in Figure 2. If the non-Hermitian eigenvalue problem is non-defective, FEAST is expected to converge and return the wanted eigenvalues associated with the B -bi-orthonormal right and left eigenvector subspaces. The convergence rate that was discussed in Section 2.3 depends on the quality of the filter to approximate spectral projector, and the size of the search subspace (hence it depends on the number of the contour points n_e , and subspace size m_0). Some of the current limitations of the algorithm are outlined in the following:

Ill-conditioned linear systems - In contrast to Hermitian FEAST which allows the selection of complex shifts (contour points) that are not located on the real axis, some of these shifts could potentially come close to a complex eigenvalue using non-Hermitian FEAST. Similar to a traditional (Hermitian or non-Hermitian) Arnoldi algorithm using shift-and-invert strategy, the resulting linear systems may become ill-conditioned. If the shift happens to be at the exact position of the eigenvalue, the linear system will also be singular. One practical solution of this problem consists of moving the contour nodes appropriately and automatically by analyzing the eigenspectrum on-the-fly.

Defective system - Currently if the system is defective, the QZ algorithm used to solve the reduced system in Step-4b of Figure 7 would not produce a set of B -bi-orthogonal subspaces. In practice, the algorithm may still be found to converge (without Step-2), but further studies are required to analyze the action of the approximate spectral projector on the Jordan form (2.1) and (2.2).

Ill-conditioned eigenvalue problem - Non-Hermitian systems are sensitive to the conditioning of the eigenvalues [15]. A well-known case is the real non-symmetric Grcar matrix [39, 9] (e.g. with $n = 100$), which gives rise to extremely sensitive eigenvalues. It appears some noticeable differences in the eigenvalue calculated using LAPACK-MATLAB, while comparing between the eigenvalue solutions of the matrix and its transpose. If double precision arithmetic is desired, this problem would require to perform the numerical operations in quad-precision [24]. Interestingly, when FEAST operates on the Grcar matrix or its transpose, the problem of sensitivity of the eigenvalues is not observed in any selected regions of the complex plane. For this matrix case, the projected reduced eigenvalue problem is then likely to be better conditioned than the original one. On the other hand, we have found that enforcing the condition of bi-orthogonality could affect the FEAST convergence for some other systems e.g. see the case of the QC2534 matrix discussed in Ref. [37]. Further studies are clearly needed to better understand the effect of ill-conditioned eigenvalue systems on FEAST.

3. FEAST Eigensolver v3.0 Outlook. The FEAST numerical library package [10] has originally been developed to address the Hermitian eigenvalue problem. The package was first released (under free BSD license) in Sep. 2009 (v1.0), followed

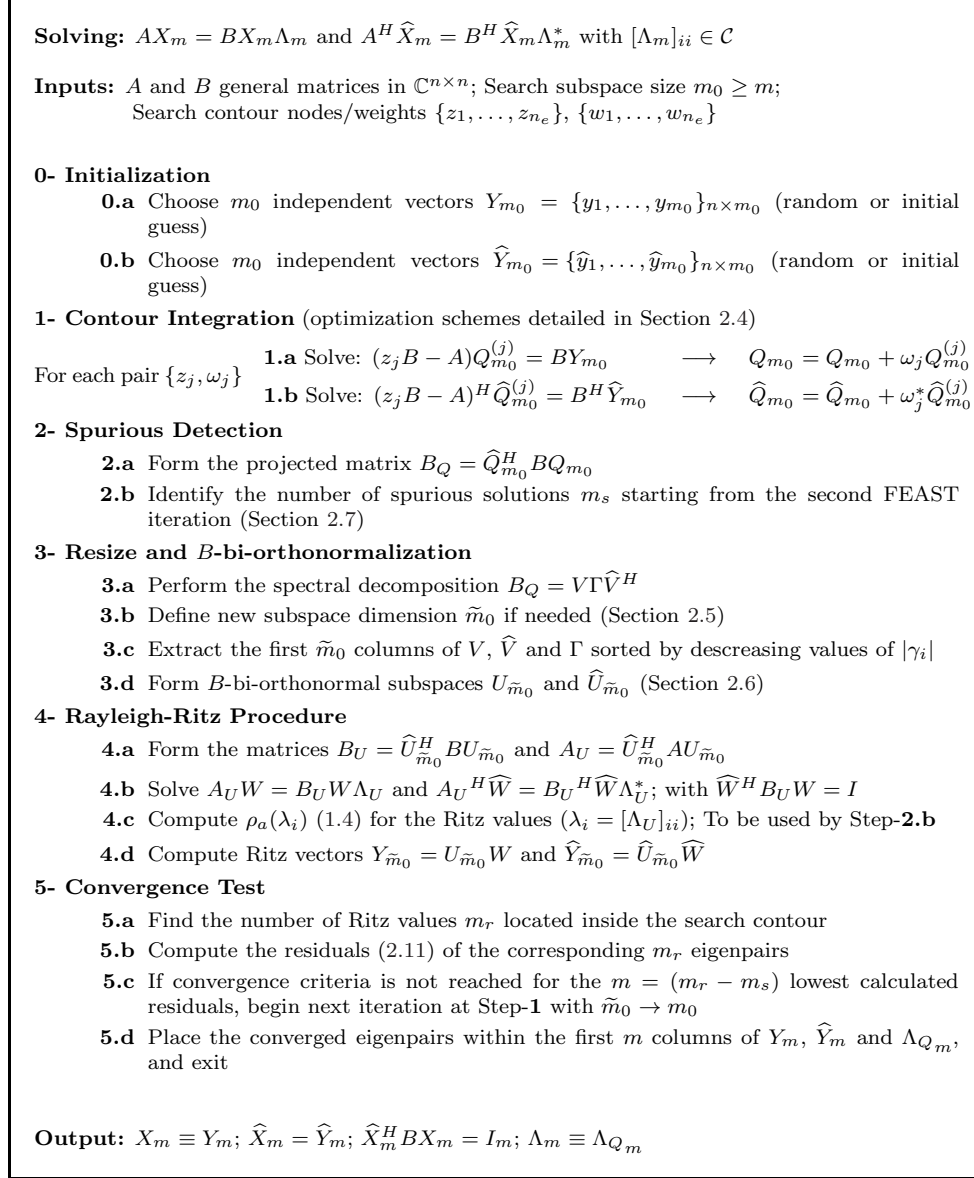


Fig. 7: FEAST Non-Hermitian general algorithm

by upgrades in Mar. 2012 (v2.0), and Feb. 2013 (v2.1). The latter was adopted by Intel math kernel library (Intel-MKL). The current version of the FEAST package (v3.0) released in Jun. 2015, started including all the various implementation of the non-Hermitian algorithm (real non-symmetric, complex symmetric, and complex general) on both shared-memory systems (i.e. FEAST-SMP version) and distributed architectures (i.e. FEAST-MPI version). FEAST's implementation exploit a key strength of modern computer architectures, namely, multiple levels of parallelism. FEAST-MPI includes the three levels of parallelism: MPI for the search contour -

MPI for the distribution of the linear systems along the contour nodes - OpenMP for the system solver.

All functionalities of FEAST are accessible through a set of standard predefined interfaces. The “ready-to-use” default drivers are capable to accept dense, banded, and sparse (CSR) matrix formats. For solving the shifted linear systems, the dense, banded, and sparse FEAST interfaces make use of LAPACK [1], SPIKE-SMP [26], and Pardiso [34] (MKL-version), respectively. For more advanced users, the FEAST library also includes features such as reverse communication interfaces (RCI) that are both matrix format and linear system solver independent. These RCI interfaces can then be customized by the end users to allow maximum flexibility for their applications. In particular, the user is in control of the three major numerical computations to perform on matrices: (i) Factorize $(z_j B - A)$ (and $(z_j B - A)^H$ if needed); (ii) Solve $(z_j B - A)Q_{m_0}^{(j)} = BY_{m_0}$ and $(z_j B - A)^H \widehat{Q}_{m_0}^{(j)} = B^H \widehat{Y}_{m_0}$; (iii) Mat-vec procedure involving the multiplications of matrices A , B , A^H , B^H with m_0 multiple vectors. In order to address very large sparse systems, customized routines such as iterative linear system solvers with or without preconditioners, or domain decomposition techniques, can straightforwardly be plugged into the RCI loop to perform these operations. Consequently, the software package has been very well received by the HPC and application developers, especially in the electronic structure and nanoelectronics communities (e.g. [6, 14, 30]).

In addition to the non-Hermitian interfaces, various supporting routines have also been added in v3.0. These includes: (i) a fast stochastic estimator that can provide a reasonable guess of the number of eigenvalues count within a user-defined search contour [8]; and (ii) a routine that can assist the user to extract nodes and weights from a custom design arbitrary geometry in the complex plane. This is particularly helpful for non-Hermitian routines as it grants flexibility in targeting specific eigenvalues.

4. Numerical Experiments. The non-Hermitian eigenvalue problem (NEP) collection [2] has been used for testing and development. Our test parameters and results for a set of selected system matrices are provided in Table 2. A subset of the eigenpairs has been targeted for each system matrix corresponding to the information provided in the NEP collection, if available. Only a few number of FEAST subspace iterations, is needed for most systems to reach convergence.

Matrix	n	m_0	m	λ_{mid}	r	#Iteration
BFW782	782	44	22	(-5300,300)	10000.0	2
BWM200	200	36	18	(-1200,0.0)	60.0	2
CDDE5	961	140	70	(4.75,0.0)	0.25	2
GRCAR	100	38	19	(0.3,0.2)	0.5	4
QC324	324	72	37	(0.0,0.0)	0.04	3
RBS480	480	112	56	(0.0,0.5)	0.5	9
RW136	136	38	19	(1.0,0.0)	0.5	5
TOLS340	340	16	8	(-60,300)	30.0	3
TOLS4000	4000	144	72	(-60,300)	233.0	8

Table 2: Non-Hermitian test cases from NEP collection. The contour is chosen as a full circle defined by the center and radius (λ_{mid}, r) using $n_e = 16$ integration points, and the criteria of convergence for the residual is set at 10^{-12} . The system size n , the subspace size m_0 , the final number of eigenvalues m found within the search contour, the final residual, and number of FEAST iterations to reach convergence are also listed.

4.1. Parallelism. As mentioned previously, a major advantage to FEAST are the multiple levels of parallelism naturally contained within the algorithm. The following results were gathered on a shared memory machine with 8 10-core Intel Xeon E7-8870 processors. Each MPI process uses 5 cores.

Multiple contours can be solved independently using the first level of parallelism of FEAST (overall orthogonality is also largely preserved [38, 11]). However, there is a threshold on the number of eigenvalues that can be calculated efficiently using a single FEAST contour. In practice m_0 should represent only a small percentage of the matrix size and it may not be suitable to go beyond few thousands because of the $O(m_0^3)$ complexity of the reduced system solve. If enough parallel resources are available, however, the solution for an arbitrary large number of eigenvalues can be obtained by partitioning the entire search domain into multiple contours. FEAST can then be applied to each in parallel with a reduced value for m_0 . An example of such partitioning is illustrated in Figure 8. The test uses the FEAST dense interfaces

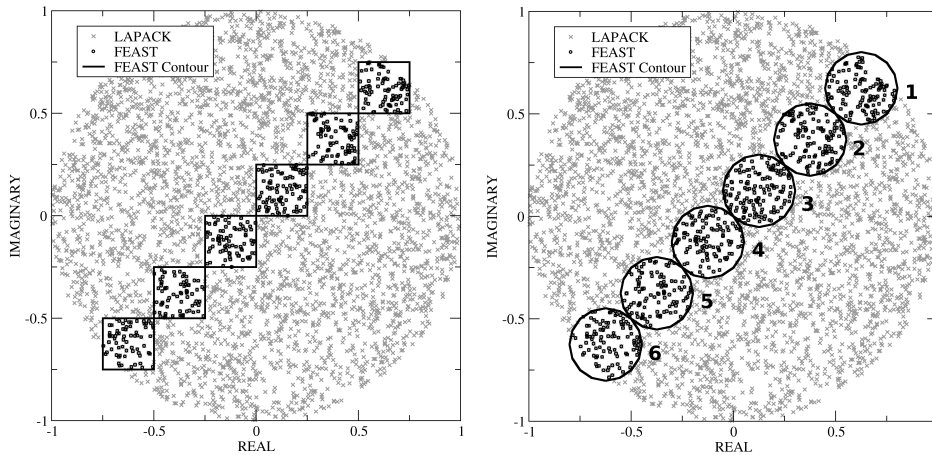


Fig. 8: A 4000×4000 dense matrix has been constructed such that all eigenvalues exist within the unit disk. Multiple FEAST contours have been used to calculate a subset of the eigenvalues in parallel.

on a 4000×4000 dense matrix constructed such that all eigenvalues exist within the unit disk. Two sets of contours are considered: First, squares with 4 trapezoidal intervals along each line segment for a total of 16 linear systems to be solved; Next, circles defined by 16 integration nodes. In all cases the size of the search subspace is set at $m_0 = 200$, and the criteria of convergence for the residual at 10^{-12} . At first we consider using only one MPI process per contour, so the 16 linear systems are solved one after another using the LAPACK dense solver. Table 3 reports the number of eigenvalues found in each contour, the number of FEAST iterations, and the total simulation times. Two simulation times are given, the fastest has been obtained using a new option offered in FEAST v3.0 that allows to save and reuse the factorization at each iteration (increasing then the memory footprint by the number of integration nodes, but removing the need to perform this costly step multiple times). Saving the factorization between FEAST iterations produced a $2 - 3 \times$ speed improvement

for all contours. As it can be observed from the number of FEAST iterations and the simulation times in Table 3, load balancing becomes an issue with some contours taking more than twice the time of the fastest converging contour. Since FEAST runs in parallel, its overall efficiency depends on the slowest converging contour (i.e Square 5 or Circle 3).

Contour N ^o	m	#Iterations	Time-1 (s)	Time-2 (s)
Square				
1	84	9	556	236
2	85	7	443	197
3	95	15	891	359
4	83	12	723	299
5	73	19	1107	438
6	69	12	718	297
Circle				
1	120	4	277	137
2	129	8	500	217
3	137	11	666	278
4	118	8	503	218
5	109	6	389	177
6	104	4	274	137

Table 3: Timing results, number of eigenvalue m and number of iterations obtained using FEAST for each contour in Figure 8, with $m_0 = 200$, $n_e = 16$ and one single MPI process per contour. Two total times are reported by contour: Time-1 for FEAST normal use, and Time-2 that does not account for the cost of the multiple matrix factorizations along the FEAST iterations which are saved in memory. We note that the overall parallel FEAST efficiency is limited by the slowest individual performance on a single contour obtained here for either Square 5 or Circle 3.

Better performances can be achieved by taking advantage of another level of parallelism for solving the set of independent linear systems. In the general case, as mentioned in Section 2.4, a single factorization and two solves must be performed at each integration node. With a total of n_e factorizations and $2n_e$ solves, the simulation time could then potentially be reduced by a factor n_e or more (since the linear systems do not need to be re-factorized at each iteration if n_e is equal to the #MPI processes). Table 4 presents scalability results for the 4000×4000 dense matrix considered in Table 3. For this small dense example, one observes only a maximum of $\sim 11 \times$ speed-up compared to a single process using 16 MPI processes. The relatively small size of the test matrix is a limiting factor since it leads to comparable times between solving a single linear system and the other numerical operations that take place in FEAST (e.g. inner product to form the reduced system, solution of reduced system, etc.). Better scalability performances could be expected using much larger sparse systems.

Conclusion. The detailed work developing the non-Hermitian FEAST algorithm has been presented. This constitutes a generalization of the well established FEAST Hermitian algorithm, leading to a significant upgrade of the FEAST solver package. The major differences between the Hermitian and non-Hermitian FEAST algorithms stem from the complex eigenvalues, which require a two-dimensional search contour. Dual subspaces are necessary to allow for computation of a B -bi-orthogonal basis of left and right eigenvectors. In order to improve the stability of the algorithm, techniques of subspace resizing, B bi-orthonormalization procedure and spurious detection

Contour N°	1	2	3	4	5	6	Speed-up
Square							
1 MPI	556	443	891	723	1107	718	1.00
2 MPI	303	231	457	370	566	368	1.96
4 MPI	160	121	244	198	303	196	3.65
8 MPI	98	88	149	132	201	128	5.51
16 MPI	56	41	70	62	95	69	11.65
Circle							
1 MPI	277	500	666	503	389	274	1.00
2 MPI	147	252	338	253	196	139	1.97
4 MPI	81	139	187	140	108	77	3.56
8 MPI	49	109	148	111	85	60	4.50
16 MPI	28	46	60	45	38	30	11.10

Table 4: MPI scalability results for the system matrix and contours considered in Figure 8 and Table 3. The first column indicated the cluster of MPI processes being used by each contour to distribute the linear systems. The last column indicates the speed-up performance associated with the slowest contour (Square 5 or Circle 3).

have been implemented and successfully tested. We note that the convergence property and parallel capability associated with the traditional FEAST algorithm have been retained with the non-Hermitian algorithm. Finally, the detailed and complete non-Hermitian FEAST algorithm implemented in v3.0 is provided, and limitations of its applicability have also been discussed.

REFERENCES

- [1] E. ANDERSON, Z. BAI, C. BISCHOF, S. BLACKFORD, J. DEMMEL, J. DONGARRA, J. DU CROZ, A. GREENBAUM, S. HAMMERLING, A. MCKENNEY, AND AND OTHERS, *LAPACK Users' guide*, vol. 9, Siam, 1999.
- [2] Z. BAI, D. DAY, J. DEMMEL, AND J. DONGARRA, *A test matrix collection for non-hermitian eigenvalue problems*, 1996.
- [3] Z. BAI, D. DAY, AND Q. YE, *Able: an adaptive block lanczos method for non-hermitian eigenvalue problems*, SIAM Journal on Matrix Analysis and Applications, 20 (1999), pp. 1060–1082.
- [4] Z. BAI AND G. W. STEWART, *Algorithm 776: Srrit: a fortran subroutine to calculate the dominant invariant subspace of a nonsymmetric matrix*, ACM Transactions on Mathematical Software, 23 (1997), pp. 494–513.
- [5] C. G. BAKER, U. L. HETMANIUK, R. B. LEHOUCQ, AND H. K. THORNQUIST, *Anasazi software for the numerical solution of large-scale eigenvalue problems*, ACM Transactions on Mathematical Software (TOMS), 36 (2009), p. 13.
- [6] S. BIRNER, T. ZIBOLD, T. ANDLAUER, T. KUBIS, M. SABATHIL, A. TRELAKIS, AND P. VOGL, *Nextnano: general purpose 3-d simulations*, Electron Devices, IEEE Transactions on, 54 (2007), pp. 2137–2142.
- [7] A. CERIONI, GENOVESE, I. DUCHEMIN, AND T. DEUTSCH, *Accurate complex scaling of three dimensional numerical potentials*, The Journal of chemical physics, 138 (2013), p. 204111.
- [8] E. DI NAPOLI, E. POLIZZI, AND Y. SAAD, *Efficient estimation of eigenvalue counts in an interval*, arXiv preprint arXiv:1308.4275, (2013).
- [9] M. EMBREE AND L. N. TREFETHEN, *Pseudospectra gateway*. <http://www.comlab.ox.ac.uk/pseudospectra>.
- [10] FEAST *Eigenolver*, 2009–2015. <http://www.feast-solver.org/>.
- [11] M. GALGON, L. KRÁMER, AND B. LANG, *The FEAST algorithm for large eigenvalue problems*, PAMM, 11 (2011), pp. 747–748.
- [12] ———, *Counting eigenvalues and improving the integration in the FEAST algorithm*, Preprint BUW-IMACM, 12 (2012), p. 22.
- [13] B. S. GARBOW, *Algorithm 535: The qz algorithm to solve the generalized eigenvalue problem*

- for complex matrices [f2], *ACM Transactions on Mathematical Software (TOMS)*, 4 (1978), pp. 404–410.
- [14] L. GENOVESE, B. VIDEAU, M. OSPICI, T. DEUTSCH, S. GOEDECKER, AND J. MÉHAUTOIS, *Daubechies wavelets for high performance electronic structure calculations: The bigdft project*, *Comptes Rendus Mécanique*, 339 (2011), pp. 149–164.
- [15] G. H. GOLUB AND C. F. VAN LOAN, *Matrix computations*, vol. 3, JHU Press, 2012.
- [16] S. GÜTTEL, E. POLIZZI, P. T. P. TANG, AND G. VIAUD, *Zolotarev quadrature rules and load balancing for the FEAST eigensolver*, to appear in *SIAM Journal on Scientific Computing (SISC)*, (2015). arXiv preprint arXiv:1407.8078 (2014).
- [17] V. HERNANDEZ, J. E. ROMAN, A. TOMAS, AND V. VIDAL, *A survey of software for sparse eigenvalue problems*, Universitat Politècnica de Valencia, Tech. Rep. STR-6, [retrieved: May, 2013]. [Online]. Available: <http://www.grycap.upv.es/slepc>, (2005).
- [18] V. HERNANDEZ, J. E. ROMAN, AND V. VIDAL, *SLEPc: A scalable and flexible toolkit for the solution of eigenvalue problems*, *ACM Transactions on Mathematical Software (TOMS)*, 31 (2005), pp. 351–362.
- [19] N. J. HIGHAM, *Functions of matrices: theory and computation*, Siam, 2008.
- [20] A. V. KNYAZEV, M. E. ARGENTATI, I. LASHUK, AND E. E. OVTCHINNIKOV, *Block locally optimal preconditioned eigenvalue solvers (BLOPEX) in hypre and petsc*, *SIAM Journal on Scientific Computing*, 29 (2007), pp. 2224–2239.
- [21] S. E. LAUX, *Solving complex band structure problems with the FEAST eigenvalue algorithm*, *Physical Review B*, 86 (2012), p. 075103.
- [22] R. B. LEHOUCQ AND J. A. SCOTT, *An evaluation of software for computing eigenvalues of sparse nonsymmetric matrices*, Preprint MCS-P547, Argonne National Laboratory, 1195 (1996), p. 5.
- [23] R. B. LEHOUCQ, D. C. SORENSEN, AND C. YANG, *ARPACK users' guide: solution of large-scale eigenvalue problems with implicitly restarted Arnoldi methods*, vol. 6, Siam, 1998.
- [24] ADVANPIX LLC., *Multiprecision computing toolbox for matlab*. <http://www.advantpix.com/>.
- [25] A. MAREK, V. BLUM, R. JOHANNI, V. HAVU, B. LANG, T. AUCKENTHALER, A. HEINECKE, H. , BUNGARTZ, AND H. LEDERER, *The elpa library: scalable parallel eigenvalue solutions for electronic structure theory and computational science*, *Journal of Physics: Condensed Matter*, 26 (2014), p. 213201.
- [26] K. MENDIRATTA AND E. POLIZZI, *A threaded SPIKE algorithm for solving general banded systems*, *Parallel Computing*, 37 (2011), pp. 733 – 741.
- [27] C. B. MOLER AND G. W. STEWART, *An algorithm for generalized matrix eigenvalue problems*, *SIAM Journal on Numerical Analysis*, 10 (1973), pp. 241–256.
- [28] B. A. PARLETT, *The symmetric eigenvalue problem*, vol. 7, SIAM, 1980.
- [29] E. POLIZZI, *Density-matrix-based algorithm for solving eigenvalue problems*, *Physical Review B*, 79 (2009), p. 115112.
- [30] QUANTUMWISE, *Atomistix toolkit version 13.8.1*. www.quantumwise.com.
- [31] Y. SAAD, *Numerical solution of large nonsymmetric eigenvalue problems*, *Computer Physics Communications*, 53 (1989), pp. 71–90.
- [32] ———, *Numerical methods for large eigenvalue problems*, vol. 158, SIAM, 1992.
- [33] T. SAKURAI AND H. SUGIURA, *A projection method for generalized eigenvalue problems using numerical integration*, *Journal of computational and applied mathematics*, 159 (2003), pp. 119–128.
- [34] O. SCHENK AND K. GÄRTNER, *On fast factorization pivoting methods for sparse symmetric indefinite systems*, *Electronic Transactions on Numerical Analysis*, 23 (2006), pp. 158–179.
- [35] D. C. SORENSEN, *Implicit application of polynomial filters in ak-step arnoldi method*, *Siam journal on matrix analysis and applications*, 13 (1992), pp. 357–385.
- [36] A. STATHOPOULOS AND J. R. MCCOMBS, *PRIMME: preconditioned iterative multimethod eigensolver methods and software description*, *ACM Transactions on Mathematical Software (TOMS)*, 37 (2010), p. 21.
- [37] P. T. P. TANG, J. KESTYN, AND E. POLIZZI, *A new highly parallel non-hermitian eigensolver*, in *Proceedings of the High Performance Computing Symposium, HPC '14, San Diego, CA, USA, 2014*, Society for Computer Simulation International, pp. 1:1–1:9.
- [38] P. T. P. TANG AND E. POLIZZI, *FEAST as a subspace iteration eigensolver accelerated by approximate spectral projection*, *SIAM Journal on Matrix Analysis and Applications*, 35 (2014), pp. 354–390.
- [39] L. N. TREFETHEN, *Pseudospectra of matrices*, Oxford University, Computing Laboratory Numerical Analysis Group, 1991.
- [40] L. N. TREFETHEN AND WEIDEMAN J. A. C., *The exponentially convergent trapezoidal rule*, *SIAM Review*, 56 (2014), pp. 385–458.

- [41] G. YIN, R. H. CHAN, AND M. YEUNG, *A FEAST algorithm for generalized non-hermitian eigenvalue problems*, arXiv preprint arXiv:1404.1768, (2014).
- [42] E. I. ZOLOTAREV, *Application of elliptic functions to questions of functions deviating least and most from zero*, Zap. Imp. Akad. Nauk. St. Petersburg, 30 (1877), pp. 1–59.